

EXTENDED ESSAY IN CHEMISTRY HL

**Release of quercetin from Fe<sub>3</sub>O<sub>4</sub> mesoporous magnetite nanoparticles (MMNPs) using external magnetic fields**

**RESEARCH QUESTION**

**How does the increase of the frequency of applied external magnetic fields increase quercetin release from the mesoporous magnetite nanoparticles, when using magnetic field system containing permanent magnet and solenoid with perm alloy core, connected to signal generator alternating current of 100 mA?**

**WORD COUNT: 3998**

Examination session: May 2019

## CONTENTS

<b>INTRODUCTION .....</b>	<b>2</b>
<b>HYPOTHESIS .....</b>	<b>6</b>
<b>Synthesis and characterization of magnetic mesoporous nanoparticles(MMNPs) .....</b>	<b>8</b>
A.Synthesis of MMNPs .....	8
<b>B.Characterization of MMNPs .....</b>	<b>9</b>
B.1. Field emission scanning electron microscope(FE-SEM) .....	9
B.2. The MMNPs size distribution.....	9
B.3. X-ray powder diffraction X-ray diffraction(XRPD) .....	9
B.4. Brunauer-Emmett-Teller(BET) analysis for MMNPs porosity determination .....	10
B.5. Magnetic characterization .....	10
B.6. Fourier-transform infrared spectroscopy(FTIR spectroscopy) .....	11
B.7. Zeta potential( $\xi$ ) of MMNPs .....	11
B.8. Release of quercetin with and without external magnetic fields .....	12
<b>RESULTS AND DISCUSSION .....</b>	<b>13</b>
C.1.Synthesis of MMNPs .....	13
C.2.1.Field emission scanning electron microscope(FE-SEM) and size distribution..	14
C.2.2.X-ray powder diffraction X-ray diffraction(XRPD) .....	15
C.2.3.Brunauer-Emmett-Teller(BET) analysis for MMNPs porosity determination...	16
C.2.4.Magnetic characterization.....	17
C.2.5. Loading of quercetin into MMNPs .....	17
C.2.5.1. UV/VIS spectroscopy .....	18
C.2.5.2. FTIR spectroscopy .....	20
C.2.6. Release of quercetin with and without external magnetic fields .....	22
<b>CONCLUSION AND EVALUATION.....</b>	<b>25</b>
<b>BIBLIOGRAPHY.....</b>	<b>28</b>
<b>ACKNOWLEDGEMENT .....</b>	<b>31</b>
<b>APPENDIX .....</b>	<b>32</b>

## INTRODUCTION

Flavonoids are a broad class of polyphenolic biomolecules, with numerous hydroxyl groups, found in a variety of fruits and vegetables. They exert various biological activities including anticarcinogenic<sup>1</sup>, anti-inflammatory<sup>2</sup> and, antibacterial activity<sup>3</sup>. Presumably they possess remarkable therapeutic potential in preventing the onset and progression of Alzheimer's disease and in promoting cognitive performance<sup>4</sup>.

The use of flavonoids has been limited due to their poor water solubility (high hydrophobicity) and chemical instability under physiological conditions(temperature,light,pH)<sup>5</sup>. Within this work, I will investigate **“How does the increase of the frequency of applied external magnetic fields increase quercetin release from the mesoporous magnetite nanoparticles, when using magnetic field system containing permanent magnet and solenoid with perm alloy core, connected to signal generator alternating current of 100 mA?”** Quercetin(Figure.1), a flavonoid from the

---

<sup>1</sup> I. L. Martins, C. Charneira, V. Gandin, J. L. Ferreira da Silva, G. C. Justino, J. P. Telo, A. J. Vieira, C. Marzano, A. M. Antunes, Selenium-containing chrysin and quercetin derivatives: attractive scaffolds for cancer therapy, *Medic. Chem.* 58 (2015) 4250–4265.

<sup>2</sup> M. M. Li, X. Q. Su, J. Sun, Y. F. Gu, Z. Huang, K. W. Zeng, Anti-inflammatory ursane- and oleanane-type triterpenoids from *Vitex negundo* var. *cannabifolia*. *J.Natural Produc.* 77 (2014) 2248–2254.

<sup>3</sup> R. Hendra, S. Ahmad, A. Sukari, M. Y. Shukor, E. Oskoueian, Flavonoid Analyses and Antimicrobial Activity of Various Parts of *Phaleria macrocarpa* (Scheff.) Boerl Fruit, *Int. J. Mol. Sci.* 12 (2011) 3422-3431.

<sup>4</sup> F. I. Baptista, A. G. Henriques, A. M. Silva, J. Wiltfang, O. A. da Cruz e Silva, Flavonoids as therapeutic compounds targeting key proteins involved in Alzheimer's disease, *ACS Chem. Neurosci.* 5 (2014) 83-92.

<sup>5</sup> H. Pool, D. Quintanar, J. D. Figueroa, C. M. Mano, J. E. H. Bechara, L. A. Godnez, S. Mendoza, Antioxidant Effects of Quercetin and Catechin Encapsulated into PLGA Nanoparticles, *J. Nanomater.* 2012 (2012) 1-12.

subgroup of flavonols<sup>6</sup> was investigated. Literature shows that upon therapeutic intervention with quercetin, significant neuroprotection and neuronal recovery can be achieved<sup>7</sup>.

A promising way to deliver poorly soluble drugs or other bioactive molecules is their incorporation within nanoparticles (NPs)<sup>8</sup>. Among different NPs, biodegradable NPs are gaining increased attention for their ability to serve as viable nanocarriers for site specific delivery of drugs within the body. They offer enhanced biocompatibility and convenient release profiles for a number of drugs, vaccines and biomolecules<sup>9</sup>.

However, lately biodegradable mesoporous NPs emerge as the ones having ideal properties for designed delivery system: effectively controlled particle size and surface chemistry; enhanced permeation, flexibility, solubility and release of therapeutically active agents<sup>10</sup>. Due to their large active surface area and high pore volume, they can host diverse molecules and as result have the highest drug-loading efficiency<sup>11</sup>. They can provide excellent physico-chemical protection from their degradation in physiological conditions, like during endogenic enzymatic activities<sup>12</sup>.

---

<sup>6</sup> M. Jazvinščak Jembrek, L. Vuković, J. Puhović, J. Erhardt, N. Oršolić, Neuroprotective effect of quercetin against hydrogen peroxide-induced oxidative injury in P19 neurons *J. Mol. Neurosci.* 47 (2012) 286-299.

<sup>7</sup> *ibid.*

<sup>8</sup> A. Baezaab, M. Colillaab, M. Vallet-Regí, Advances in mesoporous silica nanoparticles for targeted stimuli-responsive drug delivery, *Expert Opin. Drug Deliver.* 12 (2015) 319-337.

<sup>9</sup> A. Mahapatro, D. K. Singh, Biodegradable nanoparticles are excellent vehicle for site directed in-vivo delivery of drugs and vaccines, *J. Nanobiotechn.* 55 (2011) 1-11.

<sup>10</sup> D. Bennet, S. Kim, Nanotechnology and Nanomaterials in: Ali Demir Sezer "Application of Nanotechnology in Drug Delivery", 2014.

<sup>11</sup> N. Han, Y. Wang, J. Bai, J. Liu, Y. Wang, Y. Gao, T. Jiang, W. Kang, S. Wang, Facile synthesis of the lipid bilayer coated mesoporous silica nanocomposites and their application in drug delivery, *Micropor. Mesopor. Mater.* 219 (2016) 209-218.

<sup>12</sup> *ibid.*

As a control of their beneficial and superior flavonoid loading efficiency,  $\text{Fe}_3\text{O}_4$  magnetic mesoporous nanoparticles (MMNPs) were used as responsive drug carriers to specific stimuli, such as magnetic fields to release and/or deliver drugs in a therapeutically desirable manner<sup>13</sup>.

Iron oxides are widespread in nature and can be synthesized in the laboratory.

Eight iron oxides are known<sup>14</sup>, and among these, magnetite ( $\text{Fe}_3\text{O}_4$ ) is a promising candidate.

$\text{Fe}_3\text{O}_4$  (Figure.2) has the face centered cubic spinel structure, based on  $32\text{O}_2^-$  ions.  $\text{Fe}_3\text{O}_4$  differs from most other iron oxides in composition containing both divalent and trivalent iron.

$\text{Fe}_3\text{O}_4$  has a cubic inverse structure that consists of a cubic close packed array of oxide ions, where all of the  $\text{Fe}^{2+}$  ions occupy half of the octahedral sites while the  $\text{Fe}^{3+}$  are split across the octahedral and the tetrahedral sites. In stoichiometric magnetite, the ratio is equal to  $\text{Fe}^{2+}/\text{Fe}^{3+}=0.5$ .

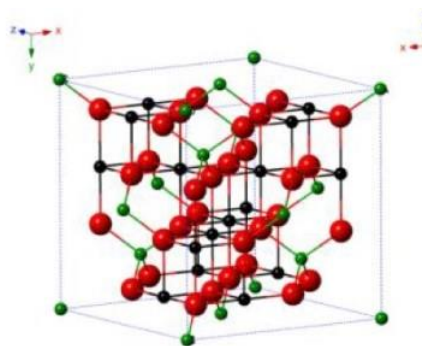
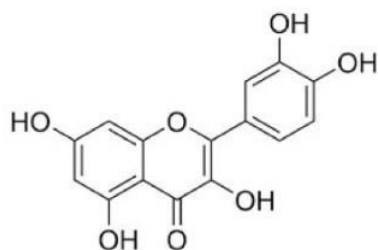


**Figure.1:**Chemical structure of quercetin **Figure.2:**Crystal structure of magnetite

<sup>13</sup> X. Z. Zhang, D. Q. Wu, C. C. Chu, Synthesis, characterization and controlled drug release of thermosensitive IPN-PNIPAAm hydrogels *Biomaterials* 25 (2004) 3793-3785.

<sup>14</sup> R. M. Cornell and U. Schwertmann, *The Iron Oxides: Structures, Properties, Reactions, Occurrences and Uses*, Weinheim: Wiley, 1996, New York.

$\text{Fe}_3\text{O}_4$  exhibits ferromagnetism at room temperature, with the saturation magnetization reaching to  $92\text{emu g}^{-1}$ .<sup>15</sup> MMNPs become superparamagnetic at room temperature when the size of crystallites within NPs is below 15nm. However, a common phenomenon observed among superparamagnetic NPs is aggregation. Therefore, it is crucial to develop a proper protection strategy to chemically stabilize bare MMNPs against aggregation during their application. For biomedical applications, it is necessary to synthesize MMNPs that are dispersible in most biological media. Functionalization by polymer provides high colloid stability, and plays a significant role in their bio-distribution<sup>16</sup>. A large number of natural and synthetic biodegradable polymers is used as functionalized material of MMNPs, but here polyethylene glycol(PEG)4000<sup>17</sup> was used.

The most decisive magnetic properties are responsiveness to outer magnetic field and magnetization, which is usually obtained from the measured hysteresis loops<sup>18</sup>(M–H) and zero-field cooled/field cooled(ZFC/FC, M–T) curves. The saturation magnetization( $M_s$ ), can be determined from the hysteresis loops. In the case of superparamagnetic MMNPs, the M–H curve does not show hysteresis, and the forward and backward magnetization curves overlap.

19

---

<sup>15</sup> M. Yamaura, R. L. Camilo, L. C. Sampaio, M. A. Macedo, M. Nakamura, H. E. Toma, Preparation and characterization of (3-aminopropyl) triethoxysilane-coated magnetite nanoparticles *J. Magn. Magn. Mater.* 279 (2004) 210.

<sup>16</sup> X. Q. Yang, J.J. Grailer, I. J. Rowland, A. Javadi, S. A. Hurley, D. A. Steeber, S. Q. Gong, Multifunctional SPIO/DOX-loaded wormlike polymer vesicles for cancer therapy and MR imaging *Biomater.* 31 (2010) 9065.

<sup>17</sup> A. J. Cole, A. E. David, J. Wang, C. J. Galbán, V. C. Yang, Magnetic brain tumor targeting and biodistribution of long-circulating PEG-modified, cross-linked starch-coated iron oxide nanoparticles *Biomater.* 32 (2011) 6291.

<sup>18</sup> hysteresis loop- a four quadrant B-H graph where hysteresis loss, coercive force and retentively of s magnetic material are obtained - "Hysteresis Loop". 24th February 2012. <https://www.electrical4u.com/hysteresis-loop/>. 20th June 2018.

<sup>19</sup> W. Wu, X. H. Xiao, S. F. Zhang, H. Li, X. D. Zhou, C. Z. Jiang, One-pot reaction and subsequent annealing to synthesis hollow spherical magnetite and maghemite Nanocages, *Nanoscale Res. Lett.* 4 (2009) 926.

An external magnetic field causes reorientation of moments of individual particle along the applied field at low temperatures. By applying an external alternating magnetic field, reorientation of the nanoparticles and increase of precession of the nanoparticles appear causing increase in drug release from nanoparticles<sup>20</sup>. The dependent variable is amount of quercetin released, the independent frequency of applied external magnetic fields and the controlled ones are time, temperature, pressure, magnet type, solenoid type, permanent magnetic field, current of 100mA, measuring devices, apparatus, reactants (concentration, volume and mass of reactants: PEG4000, PBS, EtOH, quercetin, NH<sub>4</sub>Ac, FeCl<sub>3</sub>×6H<sub>2</sub>O, ethylene glycol).

### **HYPOTHESIS:**

**Applied external magnetic fields (permanent & alternating) will increase quercetin release from MMNPs depending on their response to an external magnetic field.**

If a magnetic material is placed in a magnetic field of strength  $H$ , the individual atomic moments in the material contribute to its overall response, the magnetic induction<sup>21</sup>:

$$B = \mu_0(H + M)$$

where  $\mu_0$  is permeability of free space, and the magnetization  $M$

$$M = \frac{m}{V}$$

---

<sup>20</sup> W. Wu, X. H. Xiao, F. Ren, S.F. Zhang, C. Z. Jiang, A comparative study of the magnetic behaviour of single and tubular clustered magnetite nanoparticles J. Low Temp. Phys. 168 (2012) 306.

<sup>21</sup> Q A Pankhurst<sup>1</sup>, J Connolly<sup>2</sup>, S K Jones<sup>3</sup> and J Dobson, Applications of magnetic nanoparticles in biomedicine, J. Phys. D: Appl. Phys. 36 (2003) R167–R181.

is the magnetic moment per unit volume, where  $m$  is the magnetic moment on a volume  $V$  of the material. All materials are magnetic to some extent, but their response depends on their atomic structure and temperature. The magnetization of materials depends on their volumetric magnetic susceptibility( $\chi$ ) where

$$M = H$$

describes the magnetization induced in material by magnetic field of strength  $H$ . Upon application of a magnetic field, diamagnetic and paramagnetic materials develop negative and positive magnetization, respectively, which disappears upon removal of the field. The susceptibility gives rise to the sigmoidal shape of the  $M-H$  curve, with  $M$  approaching a saturation of magnetization at large values of  $H$ . In ferromagnetic and ferrimagnetic materials, a hysteresis appears showing an irreversibility in the magnetization process, related to intrinsic effects. The anhysteretic but still sigmoidal  $M-H$  curve is observed by superparamagnetism. Therefore, the measurement of the  $M-H$  curve can prove the superparamagnetism of the materials.

When a superparamagnetic is removed from a magnetic field, its magnetization decreases back to zero due to the ambient thermal energy of its environment. This process corresponds either to the physical rotation of nanoparticles themselves(“Brownian rotation”), or rotation of atomic magnetic moments within each nanoparticle(“Neel relaxation”). The Brownian rotation causes the reorientation of nanoparticles which caused increase in drug release from nanoparticles<sup>22</sup>.

In relation to the above-described theory of magnetization, I synthesized superparamagnetic mesoporous magnetite nanoparticles filled with quercetin. If the synthesized nanoparticles are superparamagnetic(which will be checked by measuring the M-H curve), the application of

---

<sup>22</sup> W. Wu, X. H. Xiao, F. Ren, S.F. Zhang, C. Z. Jiang, A comparative study of the magnetic behaviour of single and tubular clustered magnetite nanoparticles J. Low Temp. Phys. 168 (2012) 306.



an external alternating magnetic field will cause rotation of the nanoparticles of the same frequency as the applied external magnetic field. As the frequency of the alternating field increases, the rotation of nanoparticles will increase. The rotation of nanoparticles should be sufficiently high to overcome the adhesion and/or electrostatic forces by which the quercetin is bound to the nanoparticle surface. This will result in increased quercetin release compared to its release without the applied external alternating magnetic field.

## **METHODS<sup>23</sup>**

### **Synthesis and characterization of magnetic mesoporous nanoparticles(MMNPs)**

#### **A.Synthesis of MMNPs**

Modified solvothermal reaction was used for preparation of mesoporous magnetic nanoparticles<sup>24,25</sup>. 1.35g  $\text{FeCl}_2 \times 6\text{H}_2\text{O}$ , 3.85g of NH Ac, and 0.50g of PEG4000 Da were dissolved in 70mL of ethylene glycol. The mixture was placed in round two-necked flask, volume 250mL equipped with Graham condenser and guard tube(Figure.2-partA). Whole apparatus was placed on a hotplate-stirrer equipped with silicone oil bath. The mixture was stirred vigorously for 1h at 160°C under the protection of  $\text{N}_2$  to form a homogeneous brownish solution and then transferred into a Teflon-lined stainless-steel autoclave(Figure.2-partB) which was heated to 200°C and maintained for 16.5h. Then it was cooled to room temperature(Figure.2-partC). The black MMNPs were then rinsed three times

---

<sup>23</sup> For all materials and apparatus used observe the list of materials and apparatus in Appendix 1.

<sup>24</sup> C: C. Wang, C. Multi-Functional Thermosensitive Composite Microspheres with High Magnetic Susceptibility Based on Magnetite Colloidal Nanoparticle Clusters, *Langmuir* 26 (2010) 1674–1679.

<sup>25</sup> B. Luo, S. Xu, W. F. Ma, W. R. Wang, S. L. Wang, J. Guo, W. L. Yang, J. H. Hu, C. C. Wang, Fabrication of Magnetite Hollow Porous Nanocrystal Shells as Drug Carrier for Paclitaxel. *J. Mater. Chem.* 20 (2010) 7107–7113.

with ethanol to remove solvent. The MMNPs were separated from the supernatant by using centrifuge during each rinsing step.

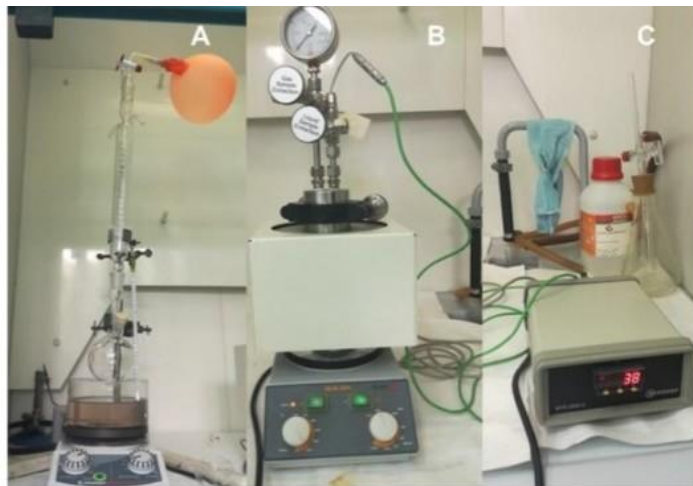


**Figure.2:** Scheme of the apparatus for synthesis of MMNPs

## **B.Characterization of MMNPs**

### **B.1. Field emission scanning electron microscope(FE-SEM)**

Field emission scanning electron microscope JSM-7000F was used for observation of particle morphology. The FE-SEM was connected to the EDS/INCA350 energy dispersive X-ray analyser for elemental analysis. Samples dispersed at an appropriate concentration were cast onto a glass sheet at room temperature and imaged.

### **B.2. The MMNPs size distribution**

The size distribution was determined using Image-J by measuring diameters of 500 NPs based on FE-SEM images and presented as a histogram of the nanoparticle diameters.

### **B.3 X-ray powder diffraction X-ray diffraction(XRPD)**

XRPD is very important in research of new materials. Here, X-ray diffraction in polycrystalline is used to determine crystalline size, crystal and amorphous material differentiation and to solve and crystallize the crystalline structure. In diffraction structural analysis, monochromatic x-ray radiation with small wavelengths is used in range from  $\lambda=0.05$  to  $0.25\text{nm}$ . Since the  $\lambda$  of X-rays approximates the size of the atoms, this radiation is suitable for determining the structural arrangement of atoms and molecules of different materials. The position of the diffraction maximum is determined by crystal grating, size and form of the unit grid, and intensity of the diffraction peak atoms of the atom and their spatial deployment in the unit cell according to the requirements of the symmetry, i.e. the crystal structure. In addition to determining the position of diffraction lines that are directly related to size and shape of the unit grid, a lot of additional information is obtained from the data which affects intensity of the individual maximum lines. The structural features of prepared sample were studied and characterized by powdered X-ray diffraction at room temperature using a Philips MPD 1880 diffractometer with monochromatic CuK $\alpha$  radiation ( $\lambda=0.1541\text{nm}$ ). All samples were recorded at angle  $2\theta$  in range of  $10\text{-}70^\circ$  with a  $0.02^\circ$  step with a fixed time of 10s per step.

### **B.4 Brunauer-Emmett-Teller(BET) analysis for MMNPs porosity determination**

Nitrogen adsorption-desorption measurements were performed on an ASAP2020 accelerated surface area analyser at  $77\text{K}$ . Before measuring, samples were degassed in a vacuum at  $120^\circ\text{C}$  for at least 6h.

### **B.5. Magnetic characterization**

To confirm the superparamagnetic property of synthesized MMNPs, magnetization measurements were performed. Magnetization of powder samples of MMNPs was measured with a MPMS-5 commercial magnetometer equipped with a superconducting quantum interferometer device (SQUID). The measurements of samples were corrected by taking into account the ampoule and temperature independent contributions. In addition, the field dependence of the magnetization ( $M(H)$ ), including magnetic hysteresis loops, was measured at temperature 290K in fields up to 10kOe.

### **B.6. Fourier-transform infrared spectroscopy (FTIR spectroscopy)**

FTIR spectroscopy is a technique used to obtain an infrared spectrum of a solid, liquid or gas. An FTIR spectrometer simultaneously collects high-spectral-resolution data over a wide spectral range. This confers a significant advantage over a dispersive spectrometer, which measures intensity over a narrow range of wavelengths<sup>26</sup>. FTIR spectroscopy is named for Fourier transform (mathematical process), required to convert raw data into the actual spectrum. FTIR spectra were measured on an ABB Bomem MB102 spectrometer, equipped with CsI optics and a DTGS detector. All spectra were collected with a nominal resolution of  $4\text{cm}^{-1}$  and 32 scans at  $25^\circ\text{C}$ . The samples were dried and mixed with KBr to be compressed to a plate for measurement.

---

<sup>26</sup> P. Atkins, L. Jones, L. Laverman, Chemical Principles, 6th Edition, W.H. Freeman and Company, 2013, New York, 105-106.

### **B.7. Zeta potential( $\zeta$ ) of MMNPs**

The zeta( $\zeta$ ) potential of MMNPs was measured using a Zetasizer Nano ZS equipped with a green laser(532nm) using the M3-PALS technique. All measurements were conducted at 25°C. Data processing was done by the Zetasizer software 6.32. Results are reported as an average value of 3 independent measurements.

### **B.8. Release of quercetin with and without external magnetic fields**

The magnetic field system was set up from permanent magnet(rare earth) and solenoid with perm alloy core at distance of approximately 7cm and connected to signal generator alternating current of 100mA(Figure.3). Among the two magnetic fields, a bottle with the sample was placed. Defining the  $O_{xy}$  plane as the surface of the liquid, the permanent field was along the  $O_z$  axis and the alternating field along the  $O_x$  axis. In all experiments weak fields were applied: the strength of the magnetic field was 0.19T. Quercetin tests the release kinetics under permanent and alternating magnetic field. Three series of measurements of 4h duration with the field having frequencies 0.1Hz, 1Hz and 10Hz and one without the field were performed.

The release of quercetin from MMNPs(60mg) placed within Standard RC Membrane in 30mL mixture EtOH/PBS (vol.50/50) was quantified by UV absorption measurements (Bio spectrophotometer,10mm quartz cuvettes) of the supernatant solution (1.5mL) during 4h. Each aliquot of measured supernatant was replaced with same aliquot (1.5mL) of fresh mixture EtOH/PBS(vol.50/50) for maintaining the volume of the supernatant constant. Temperature in the measuring compartment was controlled and maintained at 25°C. The calibration curve was drawn by dissolving different amounts of quercetin in mixture

EtOH/PBS(vol.50/50) and after filtration of supernatant through filter (F2613-3, PTFE 0.45 $\mu$ m) measuring the peak maximum in the UV absorption spectra( $\lambda_{\text{max}} = 375\text{nm}$  for quercetin). The linearity of calibration was found to be valid from  $1 \times 10^{-6} \text{mol dm}^{-3}$  to  $1 \times 10^{-4} \text{mol dm}^{-3}$  with correlation coefficients for quercetin all approaching to 1.00.

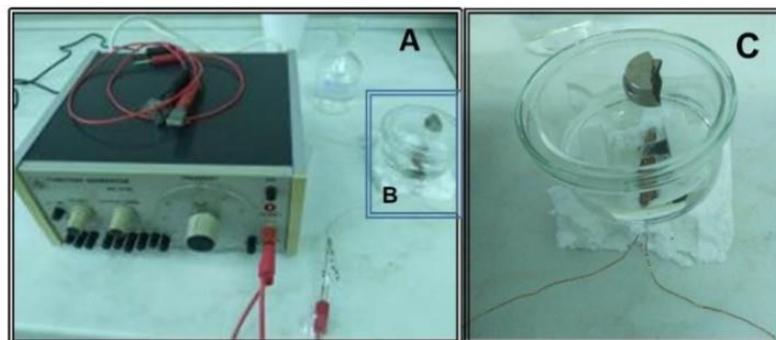


**Figure 3.** (A) Apparatus for quercetin release measurement under external magnetic fields, (B) chamber with MMNPs within the dialysis membrane under external magnetic fields; (C) zoomed figure (B)

## RESULTS AND DISCUSSION

### C.1. Synthesis of MMNPs

Solvothermal reaction was performed in the formation of submicrometer MMNPs to improve their effectiveness in drug loading and decrease costs. The Wang group described the solvothermal synthesis of magnetic clusters stabilized with poly-(acrylic acid)(PAA) which is very expensive<sup>27</sup>. Magnetic clusters with high magnetization that are able to host hydrophobic therapeutic quercetin were obtained. Therefore, this procedure was improved by replacing the PGA stabilizer with biodegradable PEG-4000, thus improving biocompatibility, decreasing

<sup>27</sup> B. Luo, S. Xu, A. Luo, W. R. Wang, S. L. Wang, J. Guo, Y. Lin, D. Y. Zhao, Mesoporous Biocompatible and Acid-Degradable Magnetic Colloidal Nanocrystal Clusters with Sustainable Stability and High Hydrophobic Drug Loading Capacity, ACS Nano 5 (2011) 1428–1435.

the costs of synthesis of MMNPs, and extending their application to hydrophobic drugs. The proposed mechanism of the synthesized MMNPs is shown on Figure.4.

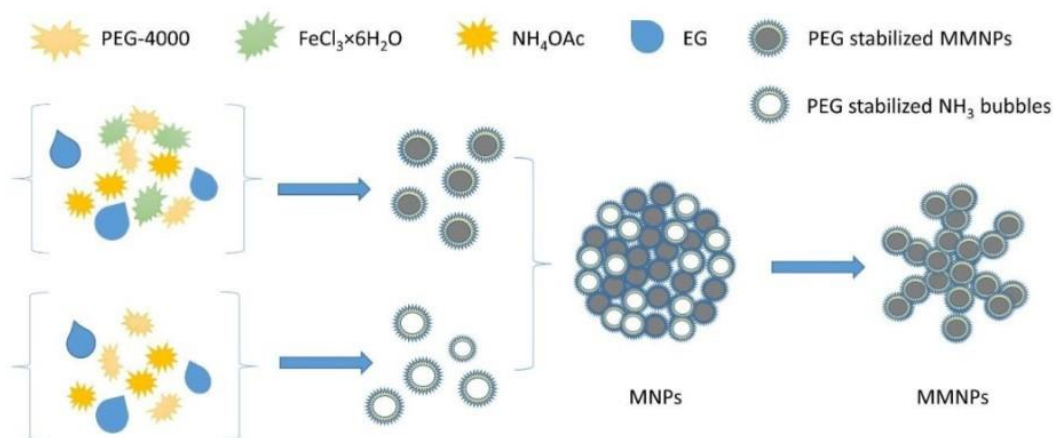


**Figure.4:** The scheme of the synthesis of the MMNPs

## C.2. Characterization of synthesized MMNPs

### C.2.1. Field emission scanning electron microscope (FE-SEM) and size distribution

As shown in Figure.4. (scheme of synthesis process) and Figure.5 (representative SEM image), the mesoporous MMNPs consisting of primary  $\text{Fe}_3\text{O}_4$  nanocrystals are almost uniform both in size and shape. The size distribution of synthesized MMNPs showed their mean size of 58nm with standard deviation of 18nm (Figure.6).<sup>28</sup>

<sup>28</sup> For the frequency table observe Table.2 Appendix 2, and for the standard deviation, highest and lowest diameters as well as mean observe Appendix 2

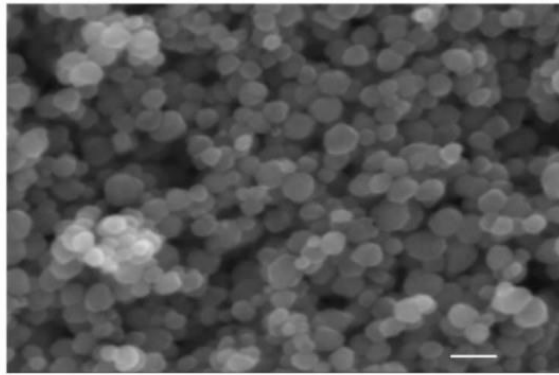


**Figure.5:** Representative SEM image of the polyethylene glycol- $\text{Fe}_3\text{O}_4$  MMNPs with scale bar of 100 nm

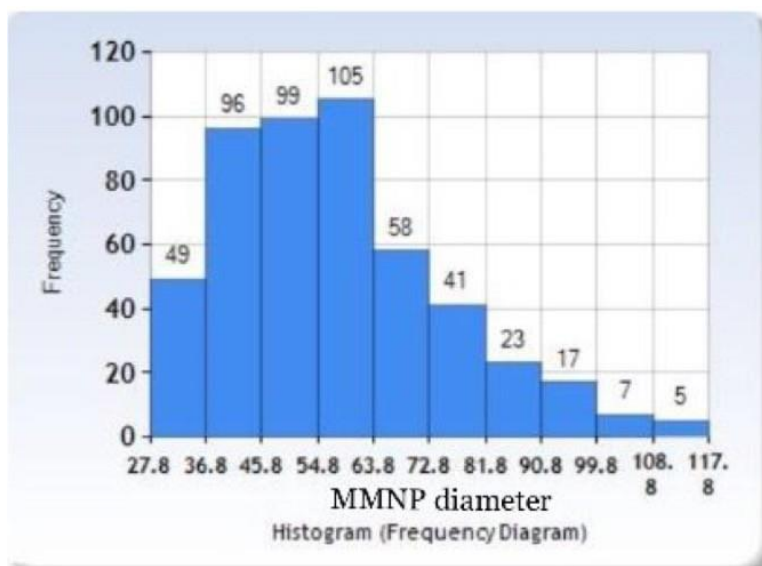


**Figure.6:** Histogram of MMNPs' diameters

## C.2.2 X-ray powder diffraction X-ray diffraction(XRPD)

The powder X-ray diffraction(XRD) patterns of the as-prepared MMNPs(Figure.7) showed



that all diffraction peaks can be well indexed to the magnetic cubic structure of  $\text{Fe}_3\text{O}_4$ <sup>29</sup> exhibiting many magnetite nanocrystals whose sizes are around 35nm.

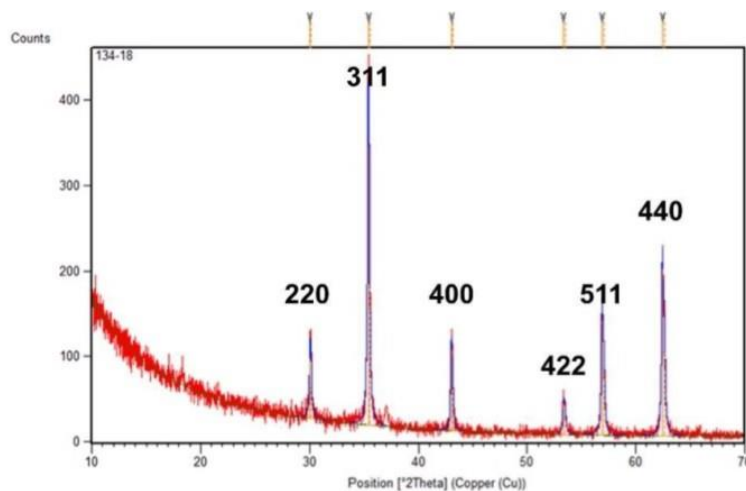


**Figure.7:** XRD pattern of MMNPs obtained with PEG 4000

### 2.3 Brunauer-Emmett-Teller(BET) analysis for MMNPs porosity determination

Nitrogen adsorption-desorption isotherms of MMNPs obtained with 500mg of PEG confirmed their mesoporosity. The BET surface area, pore size and total pore volume are calculated to be  $16.69\text{m}^2\text{g}^{-1}$ ,  $25.93\text{nm}$  and  $0.106\text{cm}^3\text{g}^{-1}$ , respectively, strongly supporting the fact that the MMNPs have mesoporous structure.<sup>30</sup>

<sup>29</sup> P. Kumar, C. Joshi, A. Barras, B. Sieber, A. Addad, L. Boussekey, S. Szunerits, R. Boukherroub, S. L. Jain, Core-shell structured reduced graphene oxide wrapped magnetically separable rGO@CuZnO@Fe<sub>3</sub>O<sub>4</sub> microspheres as superior photocatalyst for CO<sub>2</sub> reduction under visible light, Appl. Catal. B 205 (2017) 654-665.

<sup>30</sup> For experimental conditions performed under MMNPs observe Table.3 in Appendix 3

#### C.2.4 Magnetic characterization

Magnetic characterization using a magnetometer at 290K indicated that the MMNPs synthesized with 500mg PEG have saturation magnetization value of  $84.5 \text{ emu g}^{-1}$  (Figure.8). Measurement of magnetisation of synthesized MMNPs confirmed their superparamagnetic properties, thus confirming their further application in release studies under applied magnetic fields.

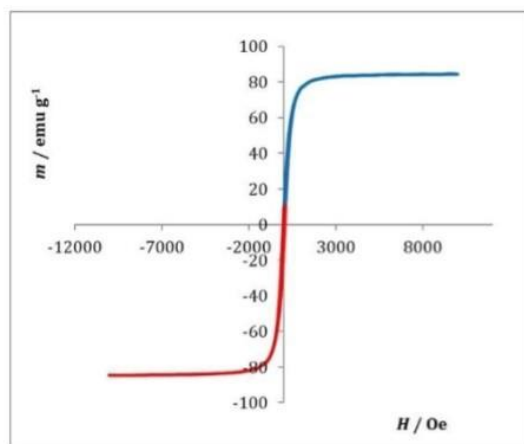


**Figure 8.** Magnetic hysteresis curve of MMNPs

#### C.2.5 Loading of quercetin into MMNPs

The significant surface area, high pore volume and pore size of synthesized MMNPs ensure access to their potential to be promising drug delivery vehicles for quercetin. Loading of quercetin was performed in pure ethanol. 30mg MMNPs was added to 30mL quercetin saturated solution. The suspension of MMNPs are stirred for 24h to allow diffusion into pores. Quercetin loaded MMNPs were separated by applying centrifuge and dried in desiccator overnight. Successful loading of quercetin was confirmed by UV/VIS spectroscopy, zeta potential measurements and FTIR spectroscopy.

### C.2.5.1. UV/VIS spectroscopy

The Beer-Lambert law<sup>31</sup> is applied to determine the amount of quercetin loaded into MMNPs. UV/VIS spectroscopy was employed to directly measure quercetin concentration loss in pure EtOH supernatant above synthesized MMNPs measuring the absorbance at wavelength  $\lambda=375\text{nm}$ . The Beer-Lambert law is the linear relationship between absorbance and concentration of an absorbing species, written as:

$$A = \epsilon bc$$

where  $A$  is measured absorbance,  $\epsilon(\lambda)$  wavelength-dependent molar absorptivity coefficient with units of  $\text{M}^{-1}\text{cm}^{-1}$ ,  $b$  path length, and  $c$  molar concentration.

Compared with quercetin concentration supernatant before adding the synthesized MMNPs, the concentration loss was determined using calibration curve in pure EtOH (Figure.9). The coefficient of determination was 0.9978, and the determined molar absorption coefficient of quercetin at temperature 298K and  $\lambda(375\text{nm})$  is  $19131\text{mol}^{-1}\text{Lcm}^{-1}$ . The loading efficiency (LE)<sup>32</sup>, the ability of the material to entrap a certain active substance is defined as<sup>33</sup>:

$$\text{Loading efficiency (\%)} = \frac{100 \times m_{\text{quercetin in MMNPs}}}{m_{\text{synthesized MMNPs}}}$$

Using this equation, the LE was determined to be  $(32.47 \pm 17.28)\%$ <sup>34</sup> calculated from 8 independent experiments shown in Table.1.

<sup>31</sup> "Beer-Lambert Law". <http://life.nthu.edu.tw/~labcjw/BioPhyChem/Spectroscopy/beerslaw.htm>, 16th November 2018.

<sup>32</sup> "Encapsulation efficiency". Research Gate.

[https://www.researchgate.net/post/How\\_do\\_I\\_calculate\\_encapsulation\\_efficiency](https://www.researchgate.net/post/How_do_I_calculate_encapsulation_efficiency), 16th November, 2018

<sup>33</sup> Notes written during the stay at the Ruder Boskovic Institute (Information given by Suzana Segota and other fellows)

<sup>34</sup> The error is displayed as a standard deviation as to be more precise. "The advantage of using  $s$  to quote uncertainty in a result is that it has the same units as the experimental data." "Chemistry Dictionary." *Chemicool*, [www.chemicool.com/definition/standard\\_deviation.html](http://www.chemicool.com/definition/standard_deviation.html).

This indicates a considerable amount of quercetin loaded into MMNPs, reflecting their potential as drug delivery carriers.

Experiment number	m (Fe <sub>3</sub> O <sub>4</sub> ) / mg ± 0.01	c (quercetin, saturated solution) / mol dm <sup>-3</sup> ± 0.00001	V (quercetin, saturated solution) / mL ± 0.1	c (quercetin, supernatant) / mol dm <sup>-3</sup> ± 0.0001	c (quercetin, loaded) / mol dm <sup>-3</sup> ± 0.00001	m (quercetin, loaded) / g ± 0.0000001	Loading efficiency / %
1	60.02	0.02407	31.5	0.0232	0.00087	0.0082827	13.75
2	60.46	0.02407	31.5	0.0220	0.00204	0.0194216	32.12
3	60.44	0.02080	31.5	0.0175	0.00330	0.0314174	51.98
4	60.24	0.02080	31.5	0.0179	0.00290	0.0276093	45.83
5	60.52	0.02140	31.5	0.0198	0.00160	0.0152327	25.17
6	60.78	0.01973	31.5	0.0183	0.00140	0.0133286	21.93
7	60.57	0.01973	31.5	0.0190	0.00080	0.0073307	12.10
8	60.14	0.02140	31.5	0.0178	0.00360	0.0342736	56.98

*Average loading efficiency = (32.47±17.28)%*

Table.1: Quercetin loadings and loading efficiency

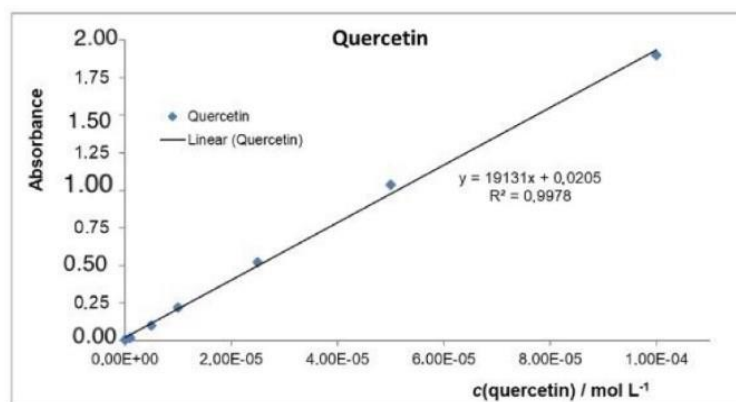


**Figure 9.** Calibration curve for determination of quercetin concentration in EtOH

### C.2.5.2. FTIR spectroscopy

Successful loading of quercetin was confirmed by FTIR spectra (Figure.10). The PEG-modified MMNPs show peak at  $1630\text{cm}^{-1}$  that may indicate the existence of Fe–O stretching and exhibit characteristic peak of magnetite at around  $581\text{cm}^{-1}$ .<sup>35</sup> Band at  $1100\text{cm}^{-1}$  indicates the presence of PEG on MMNPs<sup>36</sup>. For quercetin loaded MMNPs, bands at  $1278\text{cm}^{-1}$  and  $1179\text{cm}^{-1}$  were attributable to the C–O stretching in the aryl ether ring and the C–O stretching in phenol<sup>37</sup>.

<sup>35</sup> M. Chirita, R. Banica, A. Ieta, I. Grozescu, Unusual Behavior of Micrometric Magnetite Monodisperse Monocrystals Synthesized by Fe-EDTA Thermal Decomposition, *Particul. Sci. Technol.* 30 (2012) 354–363.

<sup>36</sup> T. P. T. Dao, T. H. Nguyen, V. V. To, T. H. Ho, T. A. Nguyen, M. C. Dang, A new formulation of curcumin using poly(lactic-co-glycolic acid)—polyethylene glycol diblock copolymer as carrier material, *Adv. Nat. Sci. Nanosci. Nanotechnol.* 5 (2014) 035013-035020.

<sup>37</sup> M. Catauro, F. Papale, F. Bollino, S. Piccolella, S. Marciano, P. Nocera, S. Pacifico, Silica/quercetin sol–gel hybrids as antioxidant dental implant materials, *Sci. Technol. Adv. Mater.* 16 (2015) 035001-035012.

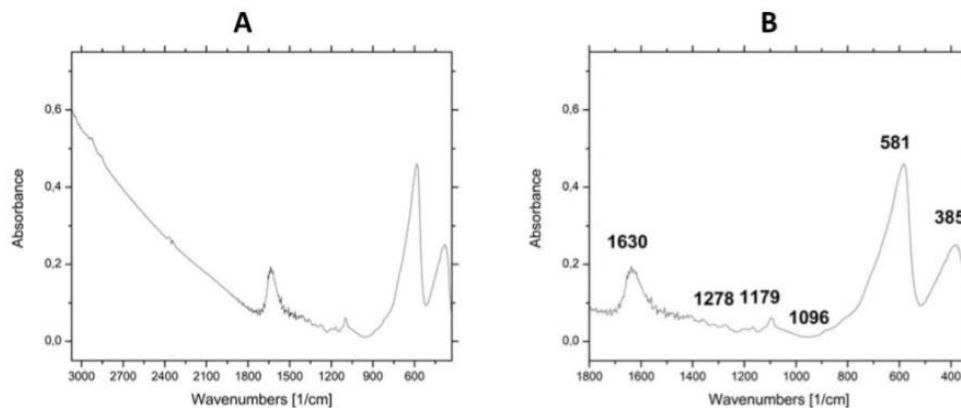


**Figure 10.** FTIR spectra of quercetin-loaded MMNPs 1) between 3000  $\text{cm}^{-1}$  and 400  $\text{cm}^{-1}$  visible in A and 2) between 1800 and 400  $\text{cm}^{-1}$  visible in B

### C.2.5.3. Zeta-potential measurements

The zeta-potential measurements for MMNPs in milli-Q  $\text{H}_2\text{O}$  at 25 °C showed that after loading quercetin, the  $\zeta$ -potential of pure  $\text{Fe}_3\text{O}_4$  MMNPs changes from negative,  $\zeta = (-22.32 \pm 0.8) \text{mV}$  ( $\text{Fe}_3\text{O}_4$ ) to less negative  $\zeta = (-17 \pm 1) \text{mV}$  ( $\text{Fe}_3\text{O}_4/\text{quercetin}$ ). The surface charge of the  $\text{Fe}_3\text{O}_4/\text{quercetin}$  is then primarily determined by the OH-groups of quercetin causing different charge potential relative to pure  $\text{Fe}_3\text{O}_4$  MMNPs. The change in  $\zeta$ -potential of MMNPs before and after their exposure to feeding solution confirms successful quercetin loading (Figure.11).

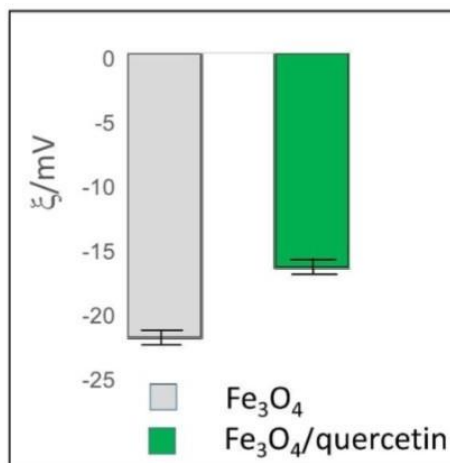


**Figure.11.** Zeta-potential of MMNPs and MMNPs with efficiently loaded quercetin in milliQ-H<sub>2</sub>O (pH 7.4). The error bars show the standard deviation between three independent samples.

### C.2.6. Release of quercetin with and without external magnetic fields

Quercetin tests the release kinetics without and under an external stimulus in the form of combination of permanent (0.19T) and oscillating magnetic fields (0.1Hz, 1Hz and 10Hz) of 4 hour duration. To determine the amount of quercetin released from MMNPs, UV/VIS spectroscopy was employed to directly measure quercetin concentration increase in supernatant mixture of phosphate buffer solution and ethanol (PBS/EtOH), volume fraction 50:50, above quercetin-loaded MMNPs measuring absorbance at wavelength  $\lambda=375\text{nm}$ . Compared with quercetin concentration in supernatant in time intervals of 4h, quercetin concentration increase was determined using calibration curve in PBS/EtOH (vol.50/50) (Figure.12). The coefficient of determination was 0.9979, and the determined molar absorption coefficient of quercetin at temperature 298K and  $\lambda=375\text{nm}$  is  $10889\text{mol}^{-1}\text{Lcm}^{-1}$ . In early stage of release, by applying alternating magnetic field 0.1Hz and 1Hz, the release of quercetin is very low and practically the same (1% after 4h). In early stage of release, a burst

was observed lasting first three hours without and by applying external stimulus in first 60min. After 120min release of quercetin reached slightly over 3% for both without external magnetic fields and for combination of permanent and alternating magnetic field of 10Hz. In last, the release was increased after 3h twofold(8%) in comparison to release without applied magnetic fields(4%)(Figure.13).

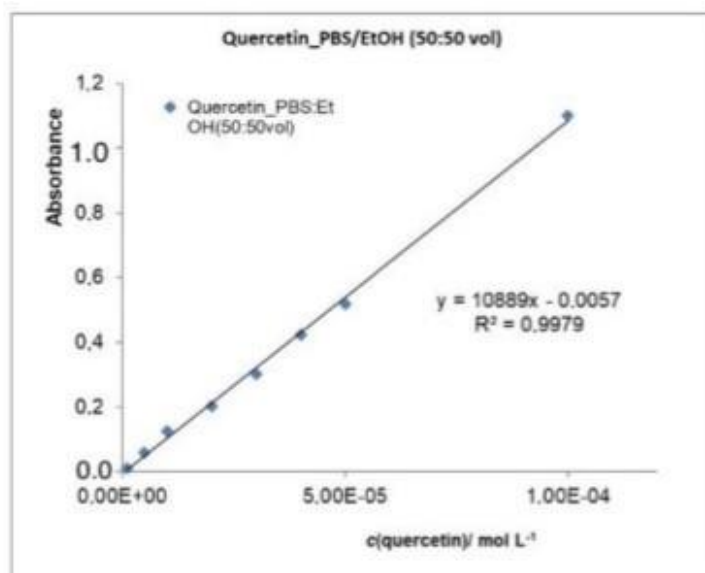


**Figure.12:** Calibration curve for determination of quercetin concentration in PBS/EtOH (50:50 vol.)



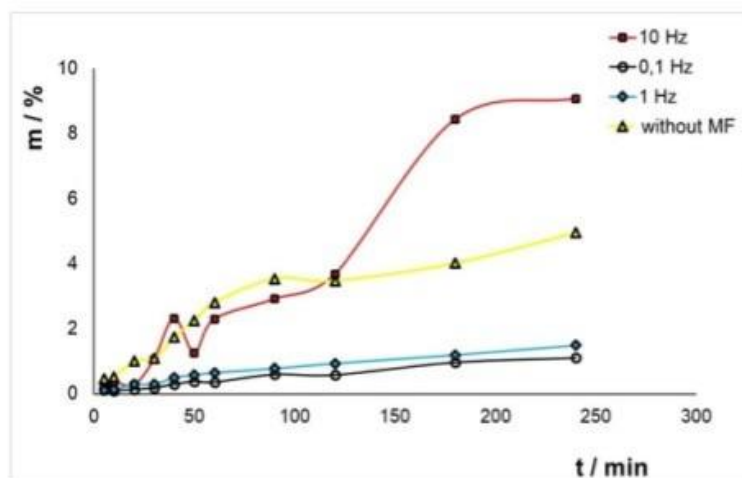


**Figure.13:** The cumulative release profile of quercetin-loaded MMNPs in PBS/EtOH (50:50 vol.) at 25 °C at 0.1 Hz, 1 Hz and 10 Hz alternating magnetic fields and without external magnetic field (MF). <sup>38</sup>

Even very low-frequency oscillating fields in combination with permanent magnetic field 0.19T significantly influence the release profiles. Strength of the permanent magnetic field and frequency of the alternating field is related to the behaviour of MMNPs in viscous medium. MMNPs rotate because of the torque due to the alternating magnetic field. The overall effect is weakening of interparticle interactions due to now enlarged interparticle distances and quicker and smoother release of the quercetin molecules from the MMNPs' interior. The rotation of the nanoparticles is supreme under relative strong permanent magnetic field of 0.19T. The final release kinetics depends on the contributions of two opposite effects. By combination of permanent magnetic field 0.19T, and alternation magnetic field of 10Hz, the release is increased, while the combinations of the same permanent magnetic field with two lower frequencies, the release kinetics were decreased. Therefore, it is demonstrated that by combining both permanent and alternating magnetic fields, fine tuning of quercetin release can be adjusted.

<sup>38</sup> For the results table look at Appendix 2.

## CONCLUSION AND EVALUATION

From the results, it was determined that the MMNPs consisting of the primary  $\text{Fe}_3\text{O}_4$  nanocrystals are almost uniform in size and shape, showing size of  $(58 \pm 18)$  nm. The powder X-ray diffraction patterns of MMNPs confirmed the magnetic cubic structure of  $\text{Fe}_3\text{O}_4$  exhibiting many magnetite nanocrystals with sizes around 35 nm. Nitrogen adsorption-desorption isotherms of MMNPs confirmed mesoporosity of MMNPs revealing the  $16.69 \text{ m}^2 \text{ g}^{-1}$  surface area, 25.93 nm pore size and  $0.106 \text{ cm}^3 \text{ g}^{-1}$  total pore volume. Measurement of magnetisation of MMNPs showed no hysteresis in M-H curve revealing saturation magnetization value of  $84.5 \text{ emu g}^{-1}$  confirming their superparamagnetic properties and further application in release studies under applied magnetic fields.

Loading of quercetin in MMNPs was confirmed by UV/VIS spectroscopy, zeta-potential measurements and FTIR. The loading efficiency is  $(32 \pm 17)\%$  indicating that a considerable amount of quercetin was loaded into MMNPs. After loading with quercetin, zeta-potential of pure  $\text{Fe}_3\text{O}_4$  MMNPs changes from negative,  $\zeta = (-22.32 \pm 0.8)$  mV ( $\text{Fe}_3\text{O}_4$ ) to less negative  $\zeta = (-17 \pm 1)$  mV ( $\text{Fe}_3\text{O}_4/\text{quercetin}$ ). The quercetin release kinetics without and under an external stimulus in the form of combination of permanent (0.19 T) and oscillating magnetic fields (0.1 Hz, 1 Hz and 10 Hz) of 4 hours' duration were examined. By applying alternating magnetic field 0.1 Hz, 1 Hz and 10 Hz, release of quercetin is increased, but the release is lower and practically the same (1% after 4h) at frequencies of 0.1 Hz and 1 Hz than release without applied external stimulus. In contrast, by applying the alternating magnetic fields of 10 Hz, in early stage of release, a burst was observed lasting first 3h without and by applying external stimulus in first 60 minutes. After 120 min release of quercetin reached slightly over 3% for both without external magnetic fields and for combination of permanent and

alternating magnetic field of 10Hz. In last, the release was increased after 3h twofold(8%) in comparison to release without applied magnetic fields(4%). Only in the case of quercetin release with combination of alternating magnetic field of 10Hz and permanent magnetic field of 0.19T is the hypothesis of increasing quercetin release confirmed, but not at the two other frequencies of 0.1Hz and 1.0Hz. However, this indicates high potential of mesoporous materials as drug carriers since MMNPs possess high magnetization, narrow size distribution, high loading efficiency and prominent biocompatibility.  $\text{Fe}_3\text{O}_4$ -MMNPs could be considered as universal and stable drug delivery material particularly able to load and release with respectable efficiency quercetin having specific physico-chemical and/or structural properties. The alternating magnetic field is neither the single nor decisive factor in release kinetics of quercetin.

The results of quercetin release from the MMNPs are in accordance with initial hypothesis. The deviations from expected results regarding quercetin release without applied alternating and permanent magnetic fields are not expected but the strength of the permanent magnetic field and frequency of the alternating field is certainly related to the behaviour of MMNPs in viscous medium. Diversely, the rotation of nanoparticles is supreme under relative strong permanent magnetic field of 0.19T. The final release kinetics thus depends on the contributions of two opposite effects.

The reason for the deviation from hypothesis could lay in the synthesis of the MMNPs since it resulted in insufficient mass of MMNPs for all experiments at once, it was necessary to repeat the synthesis several times.

Everything was performed in controlled conditions of temperature and pressure. Concentrations of all reactants were controlled. However, the synthesized MMNPs possessed chemical and structural properties that could vary. Besides, the performed experiment of the

release of quercetin from MMNPs took place in a chemistry laboratory that was temperature-conditioned. The reaction system in which MMNPs were located was not thermally insulated and stabilized. Therefore, there is a possibility of discontinuing the release medium. It is possible to repair the experimental conditions so that only the release takes place under temperature strictly controlled conditions.

An extension would include adding thermogravimetric analysis to the procedure and using other flavonoids, thus comparing the results.<sup>39</sup>

---

<sup>39</sup> View Appendix 3 for detailed extension.

**BIBLIOGRAPHY**

1. I. L. Martins, C. Charneira, V. Gandin, J. L. Ferreira da Silva, G. C. Justino, J. P. Telo, A. J. Vieira, C. Marzano, A. M. Antunes, Selenium-containing chrysin and quercetin derivatives: attractive scaffolds for cancer therapy, *Medic. Chem.* 58 (2015) 4250–4265.
2. M. M. Li, X. Q. Su, J. Sun, Y. F. Gu, Z. Huang, K. W. Zeng, Anti-inflammatory ursane- and oleanane-type triterpenoids from *Vitex negundo* var. *cannabifolia*. *J.Natural Produc.* 77 (2014) 2248–2254.
3. R. Hendra, S. Ahmad, A. Sukari, M. Y. Shukor, E. Oskoueian, Flavonoid Analyses and Antimicrobial Activity of Various Parts of *Phaleria macrocarpa* (Scheff.) Boerl Fruit, *Int. J. Mol. Sci.* 12 (2011) 3422-3431.
4. F.I. Baptista, A. G. Henriques, A. M. Silva, J. Wiltfang, O. A. da Cruz e Silva, Flavonoids as therapeutic compounds targeting key proteins involved in Alzheimer's disease, *ACS Chem. Neurosci.* 5 (2014) 83-92.
5. H. Pool, D. Quintanar, J. D. Figueroa, C. M. Mano, J. E. H. Bechara, L. A. Godinez, S. Mendoza, Antioxidant Effects of Quercetin and Catechin Encapsulated into PLGA Nanoparticles, *J. Nanomater.* 2012 (2012) 1-12.
6. M. Jazvinšćak Jembrek, L. Vuković, J. Puhović, J. Erhardt, N. Oršolić, Neuroprotective effect of quercetin against hydrogen peroxide-induced oxidative injury in P19 neurons *J. Mol. Neurosci.* 47 (2012) 286-299.
7. A. Baezaab, M. Colillaab, M. Vallet-Regí, Advances in mesoporous silica nanoparticles for targeted stimuli-responsive drug delivery, *Expert Opin. Drug Deliver.* 12 (2015) 319-337.
8. A. Mahapatro, D. K. Singh, Biodegradable nanoparticles are excellent vehicle for site directed in-vivo delivery of drugs and vaccines, *J. Nanobiotechn.* 55 (2011) 1-11.

9. D. Bennet, S. Kim, Nanotechnology and Nanomaterials in: Ali Demir Sezer "Application of Nanotechnology in Drug Delivery", 2014.
10. N. Han, Y. Wang, J. Bai, J. Liu, Y. Wang, Y. Gao, T. Jiang, W. Kang, S. Wang, Facile synthesis of the lipid bilayer coated mesoporous silica nanocomposites and their application in drug delivery, *Micropor. Mesopor. Mater.* 219 (2016) 209-218.
11. X. Z. Zhang, D. Q. Wu, C. C. Chu, Synthesis, characterization and controlled drug release of thermosensitive IPN-PNIPAAm hydrogels *Biomaterials* 25 (2004) 3793-3785.
12. R. M. Cornell and U. Schwertmann, *The Iron Oxides: Structures, Properties, Reactions, Occurrences and Used*, Weinheim: Wiley, 1996, New York.
13. M. Yamaura, R. L. Camilo, L. C. Sampaio, M. A. Macedo, M. Nakamura, H. E. Toma, Preparation and characterization of (3-aminopropyl) triethoxysilane-coated magnetite nanoparticles *J. Magn. Magn. Mater.* 279 (2004) 210.
14. X. Q. Yang, J.J. Grailer, I. J. Rowland, A. Javadi, S. A. Hurley, D. A. Steeber, S. Q. Gong, Multifunctional SPIO/DOX-loaded wormlike polymer vesicles for cancer therapy and MR imaging *Biomater.* 31 (2010) 9065.
15. A. J. Cole, A. E. David, J. Wang, C. J. Galbán, V. C. Yang, Magnetic brain tumor targeting and biodistribution of long-circulating PEG-modified, cross-linked starch-coated iron oxide nanoparticles *Biomater.* 32 (2011) 6291.
16. W. Wu, X. H. Xiao, S. F. Zhang, H. Li, X. D. Zhou, C. Z. Jiang, One-pot reaction and subsequent annealing to synthesis hollow spherical magnetite and maghemite Nanocages, *Nanoscale Res. Lett.* 4 (2009) 926.
17. W. Wu, X. H. Xiao, F. Ren, S.F. Zhang, C. Z. Jiang, A comparative study of the magnetic behaviour of single and tubular clustered magnetite nanoparticles *J. Low Temp. Phys.* 168 (2012) 306.

18. Q A Pankhurst<sup>1</sup>, J Connolly<sup>2</sup>, S K Jones<sup>3</sup> and J Dobson, Applications of magnetic nanoparticles in biomedicine, *J. Phys. D: Appl. Phys.* 36 (2003) R167–R181.
19. C: C. Wang, C. Multi-Functional Thermosensitive Composite Microspheres with High Magnetic Susceptibility Based on Magnetite Colloidal Nanoparticle Clusters, *Langmuir* 26 (2010) 1674–1679.
20. B. Luo, S. Xu, W. F. Ma, W. R. Wang, S. L. Wang, J. Guo, W. L. Yang, J. H. Hu, C. C. Wang, Fabrication of Magnetite Hollow Porous Nanocrystal Shells as Drug Carrier for Paclitaxel. *J. Mater. Chem.* 20 (2010) 7107–7113.
21. P. Atkins, L. Jones, L. Laverman, *Chemical Principles*, 6th Edition, W.H. Freeman and Company, 2013, New York, 105–106.
22. B. Luo, S. Xu, A. Luo, W. R. Wang, S. L. Wang, J. Guo, Y. Lin, D. Y. Zhao, Mesoporous Biocompatible and Acid-Degradable Magnetic Colloidal Nanocrystal Clusters with Sustainable Stability and High Hydrophobic Drug Loading Capacity, *ACS Nano* 5 (2011) 1428–1435.
23. P. Kumar, C. Joshi, A. Barras, B. Sieber, A. Addad, L. Boussekey, S. Szunerits, R. Boukherroub, S. L. Jain, Core–shell structured reduced graphene oxide wrapped magnetically separable rGO@CuZnO@Fe<sub>3</sub>O<sub>4</sub> microspheres as superior photocatalyst for CO<sub>2</sub> reduction under visible light, *Appl. Catal. B* 205 (2017) 654–665.
24. “Beer-Lambert Law”.  
<http://life.nthu.edu.tw/~labcjw/BioPhyChem/Spectroscopy/beerslaw.htm>, 16th November 2018.
25. “Encapsulation efficiency”. Research Gate.  
[https://www.researchgate.net/post/How\\_do\\_I\\_calculate\\_encapsulation\\_efficiency](https://www.researchgate.net/post/How_do_I_calculate_encapsulation_efficiency). 16th November, 2018

26. M. Chirita, R. Banica, A. Ieta, I. Grozescu, uperparamagnetic Unusual Behavior of Micrometric Magnetite Monodisperse Monocrystals Synthesized by Fe-EDTA Thermal Decomposition, *Particul. Sci. Technol.* 30 (2012) 354–363.
27. T. P. T. Dao, T. H. Nguyen, V. V. To, T. H. Ho, T. A. Nguyen, M. C. Dang, A new formulation of curcumin using poly(lactic-co-glycolic acid)—polyethylene glycol diblock copolymer as carrier material, *Adv. Nat. Sci. Nanosci. Nanotechnol.* 5 (2014) 035013-035020.
28. M. Catauro, F. Papale, F. Bollino, S. Piccolella, S. Marciano, P. Nocera, S. Pacifico, Silica/quercetin sol–gel hybrids as antioxidant dental implant materials, *Sci. Technol. Adv. Mater.* 16 (2015) 035001-035012.
29. “Hysteresis Loop”. 24th February 2012. <https://www.electrical4u.com/hysteresis-loop/>. 20th June 2018.
30. Notes written during the stay at the Ruder Boskovic Institute (Information given by Suzana Segota and other fellows)
31. “Chemistry Dictionary.” *Chemicool*, [www.chemicool.com/definition/standard\\_deviation.html](http://www.chemicool.com/definition/standard_deviation.html).

## ACKNOWLEDGEMENT

This work has been performed under the supervision of Suzana Šegota and supported by the Croatian Science Foundation, IP-2016-06-8415, to SS; <http://www.hrzz.hr/default.aspx?id=47>.<sup>40</sup>

---

<sup>40</sup> For official letter written by external supervisor view Appendix.



## APPENDIX

### APPENDIX.1.

#### LIST OF MATERIALS AND APPARATUS

In this work many apparatuses were required for the applied procedures in the previous section.

#### A) Synthesis of MMNPs

##### REAGENTS AND CHEMICALS REQUIRED:

- Ethanol, 98%, TTT d.o.o. Sveta Nedjelja, Croatia
- Iron(III) Chloride Hexahydrate, 97%, Alfa Easar, Germany
- Ammonium acetate,  $\geq 99\%$ , Fluka, Switzerland
- PEG -- Polyethylene glycol, 4000 Da,  $\geq 99\%$ , Sigma Aldrich, USA
- Ethylene glycol G.R., Lach-ner, Czechia
- Silicone oil, high temperature, Acros Organics France, 500 mL
- Deionized water (Milipore Q water)

#### B) Characterization of MMNPs

##### APPARATUS REQUIRED



- Analytical balance, Phoenix Instrument, Garbsen, Germany



- Philips MPD 1880 diffractometer with monochromatic CuK $\alpha$  radiation ( $\lambda=0.1541$  nm)



- Field emission scanning electron microscope (FE-SEM) JSM-7000F (JEOL) ASAP2020 (Micromeritics, USA) accelerated surface area analyser



- MPMS-5 commercial magnetometer equipped with a superconducting quantum interferometer device (SQUID)



- FTIR ABB Bomem MB 102 spectrometer, equipped with CsI optics and a DTGS detector  
Vortex V1 S000, IKA, Staufen, Germany



- ASAP 2020, Micromeritics, Germany

#### REAGENTS AND CHEMICALS REQUIRED

- Potassium bromide, per IR spectroscopy, Sigma Aldrich, USA
- Centrifuge-Universal 320 Hettich Zentrifugen, Tuttlingen, Germany
- Desiccator, 25 L

#### c) Loading of quercetin into MMNPs

#### REAGENTS AND CHEMICALS REQUIRED

- Ethanol, 98%, TTT d.o.o. Sveta Nedjelja, Croatia
- Quercetin-Lach-ner,  $\geq 99\%$ , Czechia

#### APPARATUS REQUIRED



- Centrifuge-Universal 320 Hettich Zentrifugen, Tuttlingen, Germany
- Desiccator, 25 L



- UV-VIS Cary 50 Spectrophotometer, Agilent Technologies, USA
- ABB Bomem MB102 spectrometer, equipped with CsI optics and a DTGS detector
- Barnstead/Lab-Line Model SHKE Max Q Mini 4450 E-Class Benchtop High



- Temperature Incubator Shaker, Connecticut, USA
- Vortex V1 S000, IKA, Staufen, Germany
- Analytical balance, Phoenix Instrument, Garbsen, Germany
- Test tubes
- Eppendorf pipettes (10  $\mu$ L, 100  $\mu$ L, 1000  $\mu$ L, 5 mL)

- Syringe Filter (F2613-3, PTFE 0,45  $\mu\text{m}$ . 17 mm), Macherey-Nagel, Germany

#### **d) Release of flavonol with and without external magnetic fields**

#### REAGENTS AND CHEMICALS REQUIRED

- Ethanol, 98%, TTT d.o.o. Sveta Nedjelja, Croatia
- Phosphate-buffered saline tablet, Sigma Aldrich, USA
- Deionized water (Milipore Q water)

#### APPARATUS REQUIRED

- Spectra/Por Closures for Standard RC Membrane MWCO 8kD 7,5/12mm,  
Spectra/Por® 6 Standard RC Pre-wetted Dialysis Tubing 8 MWCO, 1 kD, Flat  
Widths 8 mm,
- Thermostat-BTR-2000-A
- Centrifuge-Universal 320 Hettich Zentrifugen, Tuttlingen, Germany
- Desiccator, 25 L
- UV-VIS Cary 50 Spectrophotometer, Agilent Technologies, USA
- ABB Bomem MB102 spectrometer, equipped with CsI optics and a DTGS detector
- Analytical balance, Phoenix Instrument, Garbsen, Germany
- Scale
- Volumetric flask
- Test tubes
- Magnet
- Function generator, Iskra, Slovenia
- Wires
- Erlenmeyer flask, 10 mL, 25 mL, 50 mL, 100 mL
- Spatula

- Eppendorf pipettes (10  $\mu$ L, 100  $\mu$ L, 1000  $\mu$ L 5 mL)
- Syringe Filter (F2613-3, PTFE 0,45  $\mu$ m. 17 mm), Macherey-Nagel, Germany

**APPENDIX.2. Data accompanying graphs and conditions**

Frequency table	
Diameter/nm	Number of MMNPs
27.800 -- 36.799	49
36.800 -- 45.799	96
45.800 -- 54.799	99
54.800 -- 63.799	105
63.800 -- 72.799	58
72.800 -- 81.799	41
81.800 -- 90.799	23
90.800 -- 99.799	17
99.800 -- 108.799	7
108.800 -- 117.799	5

**Table.2** . MMNPs diameter data obtained using Image-J (Media Cybernetics, USA)

Additional information involving histogram (Figure 6):

- Standard deviation = 17.546
- Mean = 51.620
- Lowest Diameter = 27.873

-- Highest Diameter = 117.174

Evacuation phase		Heating phase	
The velocity of heating	10,0 °C/min	Velocity	10.0 °C/min
Temperature	100 °C	Temperature	110 °C
Velocity	1333.22 Pa/s	Time	720 min
Pressure	0.0026664473 Pa		
Time	60 min		

**Table.3.** Experimental conditions under performed MMNPs



	f = 10 Hz			f = 0.1 Hz			f = 1 Hz			f = 0 Hz		
t / min	c / mol dm <sup>-3</sup> ± 1.10 <sup>-11</sup>	m / mg ± 1.10 <sup>-7</sup>	m / %	c / mol dm <sup>-3</sup> ± 1.10 <sup>-11</sup>	m / mg ± 1.10 <sup>-7</sup>	m / %	c / mol dm <sup>-3</sup> ± 1.10 <sup>-11</sup>	m / mg± 1.10 <sup>-7</sup>	m / %	c / mol dm <sup>-3</sup> ± 1. 10 <sup>-11</sup>	m / mg± 1.10 <sup>-7</sup>	m / %
5	7.2826. 10 <sup>-7</sup>	6.6031 .10 <sup>-3</sup>	0.0929	39.3057 .10 <sup>-7</sup>	35.6388 .10 <sup>-3</sup>	0.1731	14.0509 .10 <sup>-7</sup>	12.7400 .10 <sup>-3</sup>	0.1051	18.091 7.10 <sup>-7</sup>	16.4038 .10 <sup>-3</sup>	0.4544
10	26.6324 .10 <sup>-7</sup>	24.477 9 .10 <sup>-3</sup>	0.3443	21.0304 .10 <sup>-7</sup>	20.8504 .10 <sup>-3</sup>	0.1013	18.1835 .10 <sup>-7</sup>	17.1241 .10 <sup>-3</sup>	0.1413	19.561 0.10 <sup>-7</sup>	18.5563 .10 <sup>-3</sup>	0.5140
20	19.1018 .10 <sup>-7</sup>	18.857 3.10 <sup>-3</sup>	0.2652	27.4590 .10 <sup>-7</sup>	27.6326 .10 <sup>-3</sup>	0.1342	37.5608 .10 <sup>-7</sup>	35.5181 .10 <sup>-3</sup>	0.2931	37.928 2.10 <sup>-7</sup>	36.0968 .10 <sup>-3</sup>	0.9999
30	79.9890 .10 <sup>-7</sup>	74.930 2.10 <sup>-3</sup>	1.0539	36.4588 .10 <sup>-7</sup>	37.0377 .10 <sup>-3</sup>	0.1799	36.1466 .10 <sup>-7</sup>	35.9386 .10 <sup>-3</sup>	0.2965	39.489 4.10 <sup>-7</sup>	39.2318 .10 <sup>-3</sup>	1.0868
40	175.222 7.10 <sup>-7</sup>	164.90 57.10 <sup>-3</sup>	2.3193	59.5096 .10 <sup>-7</sup>	59.5909 .10 <sup>-3</sup>	0.2894	60.8871 .10 <sup>-7</sup>	60.0098 .10 <sup>-3</sup>	0.4951	63.183 0.10 <sup>-7</sup>	62.5053 .10 <sup>-3</sup>	1.7314
50	83.3869 .10 <sup>-7</sup>	89.581 2.10 <sup>-3</sup>	1.2599	77.6012 .10 <sup>-7</sup>	78.6927 .10 <sup>-3</sup>	0.3822	78.2000 .10 <sup>-7</sup>	70.9046 .10 <sup>-3</sup>	0.5850	80.742 0.10 <sup>-7</sup>	81.2906 .10 <sup>-3</sup>	2.2518
60	159.977 9.10 <sup>-7</sup>	162.80 73.10 <sup>-3</sup>	2.2898	67.8667 .10 <sup>-7</sup>	73.3843 .10 <sup>-3</sup>	0.3564	78.5196 .10 <sup>-7</sup>	78.7576 .10 <sup>-3</sup>	0.6498	98.723 5.10 <sup>-7</sup>	101.255 0.10 <sup>-3</sup>	2.8048

90	200.936 $7 \cdot 10^{-7}$	207.19 $76 \cdot 10^{-3}$	2.9142	118.651 9 $\cdot 10^{-7}$	122.508 $4 \cdot 10^{-3}$	0.5950	92.2031 $\cdot 10^{-7}$	94.7243 $\cdot 10^{-3}$	0.7816	123.15 18. $10^{-7}$	127.880 $1 \cdot 10^{-3}$	3.5424
120	251.079 1 $\cdot 10^{-7}$	261.77 $17 \cdot 10^{-3}$	3.6817	131.876 2 $\cdot 10^{-7}$	119.573 $2 \cdot 10^{-3}$	0.5807	125.080 $4 \cdot 10^{-7}$	113.411 $4 \cdot 10^{-3}$	0.9357	138.30 47. $10^{-7}$	125.402 $0 \cdot 10^{-3}$	3.4737
180	611.718 2 $\cdot 10^{-7}$	600.14 $89 \cdot 10^{-3}$	8.4409	213.977 4 $\cdot 10^{-7}$	199.993 $7 \cdot 10^{-3}$	0.9713	153.641 $3 \cdot 10^{-7}$	144.978 $3 \cdot 10^{-3}$	1.1962	153.09 03. $10^{-7}$	145.078 $3 \cdot 10^{-3}$	4.0188
240	712.002 9 $\cdot 10^{-7}$	645.57 $88 \cdot 10^{-3}$	9.0799	251.455 6 $\cdot 10^{-7}$	227.996 $8 \cdot 10^{-3}$	1.1073	185.232 $8 \cdot 10^{-7}$	180.588 $0 \cdot 10^{-3}$	1.4900	182.47 77. $10^{-7}$	178.664 $5 \cdot 10^{-3}$	4.9492

**Table 4.** Results for quercetin release

### **APPENDIX.3. Extension**

After doing the experiment involving quercetin for my Extended Essay, the project continued with a plan to carry out the above mentioned extension. Other flavonoids including myricetin and fisetin are being used as to see how they compare to quercetin. Since they are more expensive and considered to be more promising in future treatments in the world of healthcare, the experiments will be performed with them multiple times, and the experiment with quercetin will be repeated. As the results obtained showed that the hypothesis stands for 10 Hz, future experiments could and will probably be conducted by examining the release of flavonoids when even higher frequencies are applied.

Furthermore, an extension that was performed at the institute once I was writing my Extended Essay is the thermogravimetric analysis. Thermogravimetric analysis (TGA) is a technique which measures the change in mass of polymer as a function of temperature or time under certain and controlled conditions such as atmosphere, temperature and flow. The measuring procedure is usually done in an atmosphere such as N<sub>2</sub>, He, Ar, air or O<sub>2</sub>. The TGA analysis can be performed using an isothermal or a non-isothermal method. The apparatus that records the mass change is called the thermo scale which has a bowl on which the sample is put and which then enters into a small electric oven that contains thermo element which measures the exact temperature. The instrument has to have high precision in measuring weight, temperature and time. Methods are divided into two groups: differential and integral. Non-isothermal thermogravimetric analysis results in a thermogravimetric curve that represents mass change of the sample dependent on time and temperature. This is seen on Figure 14 below and is represented with a red curve. Deriving TGA curve, differential thermogravimetric curve (DTG) is obtained, which represents the speed of mass change of the sample with temperature or time. This is seen on Figure 14 below and is represented with

a blue curve. The shape of the curve depends on the conditions of the experiment: speed of heating, shape and mass of the sample, type of gas, which flows through the oven.<sup>41</sup>

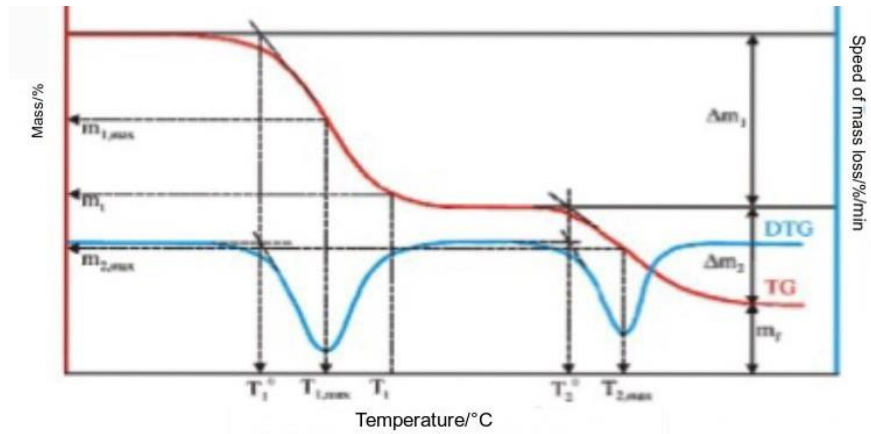


Figure.14:Thermogravimetric analysis

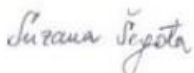
<sup>41</sup> Notes written during the stay at the Ruder Boskovic Institute (Information given by Suzana Segota and other fellows)

**Appendix.4.**

**Suzana Šegota, PhD**  
**Laboratory for Biocolloids and Surface Chemistry**  
**Department of Physical Chemistry**  
**Ruđer Bošković Institute**  
**Bijenička cesta 54**  
**Zagreb 10000**  
**e-mail: ssegota@irb.hr**  
**Zagreb, January 14th, 2019**

**RECOMMENDATION LETTER**

It is my pleasure to fill out a letter of support for Sara Dožai, student of the International Baccalaureate® (IB) Diploma Programme (DP) core in Zagreb. I met Sara Dožai in the Summer 2018, when Sara came to the Ruđer Bošković Institute for the purpose of her Extended Essay that is mandatory for all IB students. In the Summer of 2018, more specifically from 18th of June 2018 until 13th of July, Sara began to work at the Ruđer Bošković Institute in Laboratory of Biocolloids and Surface Chemistry. Sara began to work on nanostructure issues and introduced numerous spectroscopic methods for nanocharacterization of materials and surface processes within the project "Protective mechanisms and effects of nano-delivered flavonoids in model cell membranes and neurons (NanoFlavNeuroProtect)". She worked independently and followed directions when needed well. As her supervisor outside of school, I gave her all needed materials to study from and helped her with the research that needed to be done. The experiments in themselves have long methods which were designed with the help of all participants in our laboratory. During her visit, her great interest for surface chemistry as well as the practical experience in work with laboratory equipment enabled her further development and advancement in the field of chemistry, especially in physical chemistry and nanotechnology. She was one of the few students who were able to penetrate deep into the field of colloidal chemistry and techniques used in their research. Finally, Sara has an outstanding gift for team work. So far she has proven to be an extremely dedicated student with excellent understanding and clear vision of her goals. In this short time that she has spent working in our group she managed to do an extraordinary amount of work and obtain many new and interesting results. It is therefore my great pleasure to recommend Sara Dožai as a good candidate for any scholarship, which will give her a valuable opportunity to show her work to the academic world.



Suzana Šegota